Effect of Pathogenic Cysteine Mutations on FGFR3 Transmembrane Domain Dimerization in Detergents and Lipid Bilayers†

Min You,‡ Jamie Spangler,‡ Edwin Li, Xue Han, Pijush Ghosh, and Kalina Hristova*

Department of Materials Science and Engineering, Johns Hopkins University, Baltimore, Maryland 21218

Received May 22, 2007; Revised Manuscript Received July 30, 2007

ABSTRACT: Mutations in fibroblast growth factor receptors are known as the genetic basis of skeletal growth disorders. The mechanism of pathogenesis, as determined by mutation-induced changes in receptor structure, interactions, and function, is elusive. Here we study three pathogenic Cys mutations, associated with either thanatophoric dysplasia or achondroplasia, in the TM domain of fibroblast growth factor receptors 3 (FGFR3). We characterize the dimerization propensities of the mutant TM domains in detergents and in lipid bilayers, in the presence and absence of reducing agents, and compare them to previous measurements of wild-type. We find that the Cys mutations increase the propensity for dimerization in detergent, with the Cys370 mutant exhibiting the highest propensity for disulfide bond formation, the Cys371 mutant having an intermediate propensity, and Cys375 the lowest. Thus, disulfide bonds readily form in detergents, with efficiency that correlates with the severity of the phenotype. In lipid bilayers, however, the Cys370 mutant, which dimerizes strongly in detergent, behaves as the wild-type, suggesting that Cys370-mediated disulfide bonds do not form between the isolated TM domains in bilayers. Thus, the nature of the hydrophobic environment plays an important role in defining the structure and flexibility of transmembrane dimers. These results and previous findings from cellular studies lead us to propose a conformational flexibility mechanism of receptor stabilization as a basis for disregulated FGFR3 signaling in thanatophoric dysplasia and achondroplasia.

Receptor tyrosine kinases (RTKs[1]) are type I transmembrane proteins that have three domains: an N-terminal extracellular domain involved in ligand recognition and binding; a TM domain; and a catalytic tyrosine kinase domain at the C-terminus (*1*, *2*). Signal transduction occurs upon ligand (growth factor) binding to the receptor, which induces a conformational change in the extracellular domain and stabilizes the dimeric state of the receptor (*3*−*7*). The contact between the two cytoplasmic domains triggers signaling cascades, which begin with the intermolecular autophosphorylation of the receptor subunits. Therefore, enhancement in RTK dimerization propensities leads to unregulated signaling and pathologies (*8*).

RTK TM domains appear to be critical for the dimerization process. The TM domains of ErbB1, 2, 3, and 4 and of FGFR3 have a tendency for sequence-specific dimerization in membranes in the absence of extracellular domains and ligands (*9*, *10*). Furthermore, amino acid mutations in the TM domains can lead to pathologies, believed to occur due to direct stabilization of the mutant dimers through specific interactions such as hydrogen bonds (*8*). For instance, an Ala391→Glu mutation in the TM domain of FGFR3, an RTK that is critical for skeletal development, increases FGFR3 dimer stability by −1.3 kcal/mol, most probably due to the formation of Glu-mediated hydrogen bonds (*11*).

Here we investigated if disulfide bond formation between mutant Cys residues in the TM domain of FGFR3 can stabilize the dimer in a manner which is similar to the hydrogen bond-mediated stabilization. The studied Cys mutations have been associated with skeletal dysplasias. In particular, the Gly370→Cys and Ser371→Cys mutation have been linked to thanatophoric dysplasia (TD), characterized by severe shortening of the limbs, macrocephaly, and a narrow thorax with small ribs. The incidence of TD is 1 in 10,000−35,000, and it is always lethal in the neonatal period, with death occurring due to respiratory insufficiency as a result of reduced thoracic capacity or compression of the brainstem (*12*). The mutation Gly375→Cys in FGFR3 TM domain has been identified in some cases as a cause for achondroplasia, a much less severe form of human dwarfism (*13*, *14*). Achondroplasia is characterized by short arms and legs, diminished muscle tone, large head with a prominent forehead, and trident-shaped hands; its incidence is 1 in 7,000−15,000 live births.

Here we characterized the stability of the FGFR3 TM domain dimer in the presence of the Cys370, Cys371, and Cys375 mutations, in the presence and absence of reducing agents. In detergents, we observed a large dimer fraction in the absence, but not in the presence of the reducing agent, suggesting that the dimer is stabilized by disulfide bonds. We further observed a difference in the extent of dimerization

† This work was supported by Research Scholar Grant No. RSG-04-201-01 from the American Cancer Society to K.H.

* Corresponding author. E- mail: kh@jhu.edu. Phone: 410-516-8939. Fax: 410-516-5239.

‡ Contributed equally to this work.

[1] Abbreviations: FRET, Förster resonance energy transfer; TM, transmembrane; RTK, receptor tyrosine kinase; FGFR3, fibroblast growth factor receptor 3; POPC, 1-palmitoyl-2-oleoyl-*sn*-glycero-3-phosphocholine; HFIP, hexafluoroisopropanol; SDS−PAGE, sodium dodecyl sulfate−polyacrylamide gel electrophoresis.

10.1021/bi700986n CCC: $37.00
Published on Web 09/11/2007

wild-type: DEA**G**SVYAGILSYGVGFFLFILVVAAVTL**C**RLR

TM^{370C}: DEA**C**SVYAGILSYGVGFFLFILVVAAVTL**A**RLR
TM^{371C}: DEAG**C**VYAGILSYGVGFFLFILVVAAVTL**A**RLR
TM^{375C}: DEAGSVYA**C**ILSYGVGFFLFILVVAAVTL**A**RLR

$TM^{370/396C}$: RRA**C**SVYAGILSYGVGFFLFILVVAAVTL**C**RLR

FIGURE 1: Sequence of wild-type FGFR3 TM domain and the TM peptides used in this study. The Gly370→Cys mutation in TM^{370} and the Ser371→Cys mutation in TM^{371} have been associated with thanatophoric dysplasia, a lethal skeletal disorder, while the Gly375→Cys mutation in TM^{375} has been linked to achondroplasia, a much milder form of human dwarfism. Cys396 in TM^{370}, TM^{371}, and TM^{375} has been substituted with Ala to prevent 396-mediated disulfide bond formation (see text for rationale). In $TM^{370/396}$, fluorescent dyes are attached to Cys396, a residue which has been shown to not play a role in the dimerization process under reducing conditions (*10*, *15*). Cys370 and Cys396 face a very different environment under biological conditions: Cys370 faces the reducing environment of the cytoplasm, while Cys370 faces extracellular space and thus could participate in disulfide bonds. The two negatively charged residues (DE) at the N-terminus are substituted with two Arg in $TM^{370/396}$. This substitution has no effect on the dimerization of FGFR3 TM domain in detergents or in lipid bilayers (*11*, *15*); dimerization has been shown to be mediated by van der Waals knob-into-hole packing interactions of hydrophobic amino acids, not the terminal charges. Previous FRET measurements of FGFR3 dimerization have been performed with variants carrying the RR N-terminal substitution, because this substitution allows the effective separation of dyes and peptides over an ion exchange column prior to HPLC purification (*8*, *18*, *35*).

of the three mutants in the absence of the reducing agent, in a manner that generally correlates with the severity of the phenotype.

Next, we characterized the dimer stability of the Cys370 mutant (the mutant that dimerizes most extensively in detergent) in lipid bilayers, in the presence and absence of a reducing agent. The dimerization propensity of the Cys370 mutant did not depend on the presence of a reducing agent, and was exactly the same as for the previously characterized wild-type FGFR3 TM domain (*10*, *11*). Thus, disulfide bonds did not form in the model lipid bilayer, despite the fact that they formed in detergent. Here we explain these findings in terms of a high flexibility of the TM dimer structure in detergent, but a much more constrained inflexible structure in lipid bilayers. We also propose a model for disulfide bond-mediated pathogenic FGFR3 stabilization in plasma membranes, which reconciles our findings in detergents and bilayers with previous results obtained from cellular studies.

MATERIALS AND METHODS

Peptide Synthesis. The sequence of the wild-type FGFR3 TM domain and the peptides synthesized for the current study are shown in Figure 1. All peptides were synthesized via solid phase peptide synthesis using 433A ABI synthesizer (Applied Biosystems) and 9-fluorenylmethoxy-carbonyl (F-Moc) chemistry as described (*15*). Protected amino acids used included Arg(Pbf), Cys(trityl), Asp(*t*-butyl), Glu(*t*-butyl), Ser-(t-butyl), Thr(*t*-butyl), and Tyr(*t*-butyl) (Advanced ChemTech, Louisville, KY). The capping reagent contained 19 mL of acetic anhydride mixed with 9 mL of DIEA and 6 mL of a 1 M solution of HOBt in NMP, and 366 mL of NMP. The peptides were grown on a CLEAR-amide resin, 100−200 mesh (Peptides International, Louisville, KY).

To optimize yield by limiting peptide interactions on the resin, a reduced resin loading protocol was used. This modified protocol involved the addition of less than 1 equiv of the first amino acid to the resin. The coupling was permitted to occur for the standard interval and was terminated by washing the resin with NMP. The unreacted sites were acetylated using a solution of acetic anhydride and HOBt. The resin loading was thus reduced by up to 50%, such that only highly exposed sites on the resin were able to react with the first amino acid in the sequence, allowing synthesis to occur only at these select sites. Following the coupling of the first amino acid to the resin, each subsequent amino acid was coupled using a double or triple coupling protocol to enhance yield. Specifically, all residues were double coupled with the exception of the three Phe residues and the YVAGI region at the N-terminal end of the sequence, both of which have been documented to have particularly low coupling yields. After the addition of each amino acid, the unreacted sites were all acetylated to prevent coupling at these locations.

There is a naturally occurring cysteine in the sequence of wild-type FGFR3, close to the N terminus and thus facing the cytoplasm in the cell. The intracellular environment is reducing, and this residue is not expected to participate in disulfide bonds. In our previous studies of wild-type FGFR3 TM domain dimerization, the fluorescent dyes were attached to this residue; the attached dyes did not affect dimerization (*15*). In the three peptides TM^{370}, TM^{371}, and TM^{372}, wild-type Cys396 was substituted with alanine, which does not have disulfide capabilities, in order to prevent the formation of Cys396-mediated disulfide bonds in oxidizing environments. This Cys−Ala substitution is not expected to affect the dimerization propensity of the peptide, since Cys396 does not participate in the dimer interface and even attaching a dye to it does not perturb dimerization (*10*, *15*).

While the peptides TM^{370}, TM^{371}, and TM^{372}, with Cys396 substituted with Ala, were used in SDS−PAGE experiments, the dimerization studies in bilayers using FRET were carried out with the peptide $TM^{370/396}$, which contained two cysteines, Cys370 and Cys396. For the FRET studies, fluorescein or rhodamine (a FRET pair) was attached to Cys396, as described previously (*10*), while Cys375 was left unprotected and with disulfide bonding capabilities. To synthesize $TM^{370/396}$, Cys(trityl) was used for position 396, and Cys-S-acetoamidemethyl (Acm) was used for position 370. Thus, Cys396 was deprotected during cleavage and subsequently labeled with fluorescein or rhodamine. After Cys396 labeling, the Acm group was removed to yield free Cys370.

Labeling of $TM^{370/396}$. A 1 mM solution of dye (fluorescein-maleimide or rhodamine-maleimide) in MeOH was added to 100 μM peptide in HFIP. 10 mM PO_4 phospahate buffer, 100 mM NaCl was subsequently added into the mixture to a final volume ratio of HFIP/MeOH/buffer of 1:1:2. The mixture was incubated at room temperature with frequent shaking for the first 30 min, and kept in the refrigerator overnight, such that the maleimide group of the dye could react with the free Cys396. After that, *N*-ethylmaleimide was added into the mixture to cap the unreacted thiol groups, and then the mixture was incubated overnight. The rationale behind this step is that *N*-ethylmaleimide, which is much smaller than the dye, will react readily with Cys396, such that any free Cys396 left will be capped at the end of this step. Excess dye was removed over an ion exchange column and the solution was dried using a rotary evaporator.

Cleavage/Deprotection. Once synthesized, the peptides were cleaved from the resin and deprotected using trifluoroacetic acid (TFA) and ethane 1,2-dithiol (EDT) (Aldrich Chemical C., Milwaukee, WI) as cleavage and scavenger agents, respectively. For each peptide, approximately 500 mg of the vacuum-dried resin was dissolved in 500 μL of EDT and reacted for 3 min. Subsequently, 9.5 mL of TFA was added to the solution and the cleavage reaction was allowed to proceed for 90 min. Following cleavage, the peptide was precipitated from the solution with 35 mL of diethyl ether. The ether was removed, and the peptide was dissolved in 70% acetonitrile/30% water (liquid/liquid) and lyophilized. The molecular weight of the crude peptides was confirmed using MALDI-TOF analysis using an Applied Biosystems Voyager DE-STR mass spectrometer.

Removal of the ACM Group in TM$^{370/396}$. The dried peptides were dissolved in cold TFA at a ratio of 200 μL per 1 μmol of peptide. Anisol (4 μL per 1 μmol of peptide) and silver salt (AgOTf) (20× equi per Acm group) were added to the solution. The mixture was stirred at 4 °C for 1.5 h. Cold ether (8−10-fold excess) was added to precipitate the peptide silver salt. After centrifugation, the precipitated peptide silver salt was suspended in 1 M aqueous acetic acid/HFIP (1:1 ratio) containing DTT (40 equiv per Acm group). The solution was incubated at room temperature for 3 h before centrifugation. The supernatant containing the labeled peptide was lyophilized. The dried peptide was dissolved in HFIP/water (1:2 ratio) for further purification using HPLC.

Peptide Purification. The peptides were purified using reverse phase high performance liquid chromatography (HPLC) on a Vydac 214TP54 C4 column using a water/acetonitrile solvent profile (solvent A, water with 0.1% TFA; solvent B, acetonitrile with 0.1% TFA). The standard method employed for HPLC was as follows: the column was equilibrated with 30% B for 5 min, the column experienced a 25 min ramp from 30% to 100% B, the column was exposed to 100% B for 15 min, the percentage of B was reduced from 100% to 30% over the course of 5 min, and the column was kept at 30% B for 5 min. The absorbance of the peptide was monitored at 220 nm, and the purified peak was collected. After the peptides had been purified via reverse phase HPLC, the molecular weights of the purified peptides were again confirmed using MALDI-TOF mass spectrometry. The purified peptides were stored in stock solutions of methanol:HFIP (2:1). Their concentration was determined via absorbance detection of the tyrosine residues using a UV−vis Cary 50 (Varian) spectrophotometer.

Circular Dichroism. The helicity of the peptides was measured using circular dichroism (CD) spectrometry. The peptides were dissolved in MeOH/HFIP (2:1 ratio), and their helicity was characterized using a Jasco 710 spectropolarimeter as described (*10*).

SDS−PAGE The SDS−PAGE analysis involved the use of two different types of gels: 10−20% Novex tricine precast gels and NuPAGE Novex 10% Bis-Tris gels (Invitrogen, Carlsbad, CA).

Samples for the 10−20% tricine gels were 4 nmol of peptide dissolved in 4% SDS and Tris buffer (pH = 8.1). Reduced samples contained 2.5 mmol of 1,4-dithiothreitol (DTT). Samples were boiled for 5 min prior to loading in the XCell *Surelock* Mini-Cell electrophoresis apparatus (Invitrogen, Carlsbad, CA). Gels were run in tricine SDS running buffer (4% SDS, pH = 8.1) at 125 V for 90 min. They were then fixed in a 5:4:1 water:methanol:glacial acetic acid solution for 90 min, stained for 45 min with a Coomassie Blue dye solution, and destained in the same solution that was used for fixing.

The NuPAGE 10% Bis-Tris gels were run at neutral pH. For each nonreduced sample, 4 nmol of peptide was dissolved in 5 μL of LDS NuPAGE sample buffer and 15 μL of deionized water. Reduced samples, which were run on separate gels, contained 4 nmol of peptide, 5 μL of LDS NuPAGE sample buffer, 2 μL of NuPAGE reducing agent (1 μmol of DTT for 4 nmol of peptide in a lane), and 13 μL of deionized water. All samples were boiled for 5 min prior to loading. Both the reduced and nonreduced gels were run in the NuPAGE SDS running buffer in the XCell *Surelock* Mini-Cell electrophoresis apparatus, but for the reduced gels, the apparatus also contained 500 μL of NuPAGE antioxidant. The gels were run at 200 V for 35 min and fixed in the same solution used for the tricine gels for approximately 90 min. These gels were then stained for 60 min with silver stain (Invitrogen, Carlsbad, CA).

In some cases, gels were run in the presence of Cu^{2+} ions, which have been shown to be the most effective metal ions in catalyzing the oxidation of sulfhydryl groups (*16*). In these experiments, 2 μmol of $CuSO_4$ were added to nonreduced samples containing 4 nmol of peptides. In some cases, the samples were incubated overnight at pH = 10 prior to running on the gel.

Preparation of Vesicles . 1-Palmitoyl-2-oleoyl-*sn*-glycero-3-phosphocholine (POPC) was purchased from Avanti. Lipids and proteins were first mixed in HFIP/chloroform. Solvents were removed under a stream of nitrogen gas, and the mixture was lyophilized and then redissolved in 10 mM phosphate buffer, 100 mM NaCl, pH 7. The final lipid concentration was 0.25 mg/mL. The ratio of peptides to lipids was 1 to 500. Samples were then freeze−thawed several times prior to the FRET measurements. Details about sample preparation were given in ref *17*.

In some experiments, a stock of $CuSO_4$ was added to the peptide/lipid mixture prior to rehydration. The final concentration of $CuSO_4$ was 1 mM.

Förster Resonance Energy Transfer (FRET). FRET experiments in vesicles were carried out using a Fluorolog fluorometer (Jobin Yvon). To measure the FRET efficiency between fluorescein- and rhodamine-labeled TM domains, the excitation wavelength was set at 439 nm, and emission spectra were collected from 450 nm to 750 nm. FRET was measured in liposomes containing known concentrations of donor- and acceptor-labeled proteins as previously described in detail (*10*, *17*). Energy transfer, *E*, was calculated from measurements of donor intensity at 519 nm in the absence and presence of the acceptor (*10*).

Dimer Fraction Calculation. The measured FRET efficiencies were corrected for FRET arising due to random colocalization of donors and acceptors as discussed (*10*, *17*). The Förster radius of this FRET pair, needed for this calculation, has been previously measured as 56 Å (*11*). The corrected FRET efficiency is a measure of [D]/(2[D] + [M]) (0.5 × fraction of peptides in the dimeric state), where [D] is the dimer fraction in the lipid vesicles (dimers per lipid) and [M] is the monomer fraction in the lipid vesicles

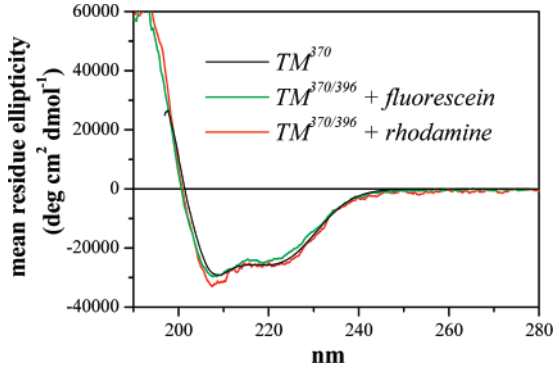

FIGURE 2: Solution CD spectra of TM^{370} (black), fluorescein-labeled $TM^{370/396}$ (green), and rhodamine-labeled $TM^{370/396}$ (red) in HFIP/methanol. All peptides shown in Figure 1 are helical, similar to the wild-type peptide (*10*, *11*) and two previously characterized pathogenic mutants (Ala391Glu and Gly380Arg) (*11*, *18*). The dyes do not affect the helicity of the peptide.

(monomers per lipid). Further details for the calculation of the dimer fraction [D] are given in refs *11*, *17*, and *18*.

Molecular Modeling. A previously published model structure of wild-type FGFR3 TM domain (*11*) was used as the starting point for model development. The wild-type model was created using the software CHI (i.e., "CNS searching of helix interactions") in vacuum (dielectric constant = 1), as previously described (*11*, *19*−*21*). Residues 370, 371, and 375 in the wild-type dimer structure were then substituted with cysteines using VMD (*22*). The final mutant dimer structures are shown in Figure 5.

We note that the wild-type dimer structure, used as a basis for the cysteine mutant model development, is consistent with some limited mutagenesis studies (*11*, *23*). Thus, the overall features and trends shown in Figure 5 are likely correct. However, the *exact* rotomer conformations and positions of the highlighted cysteines should not be overinterpreted.

RESULTS

SDS−*PAGE*. The peptides TM^{370}, TM^{371}, and TM^{375} (see sequences in Figure 1) were synthesized and purified as described in Materials and Methods. All peptides were helical in all hydrophobic environments, as shown for TM^{370} (as well as $TM^{370/396}$, see below) in organic solvent in Figure 2. The measured mean residue ellipticities for all peptides were about ∼27,000 deg cm^2/dmol in organic solvent and about ∼24,000 deg cm^2/dmol in SDS, identical to values measured for the wild-type (*10*).

To investigate the propensity for disulfide bond formation and dimer stabilization in detergent micelles, we subjected the three peptides, TM^{370}, TM^{371}, and TM^{375}, to SDS−PAGE in the presence and absence of reducing agents, as described in Materials and Methods. The SDS−PAGE results are shown in Figures 3 and 4.

On all gels, two bands could be distinguished: a monomer band with a molecular weight of around 3.5 kDa and a dimer band corresponding to a molecular weight of approximately 7 kDa. No higher order aggregates were observed on the gels, similar to published results for the wild-type and two pathogenic mutants (*11*, *18*), suggesting that only monomers and dimers of FGFR3 TM domain coexist in detergent.

On the tricine gels, 370 dimerized extensively in the oxidized state, but the dimer fraction decreased in the reduced

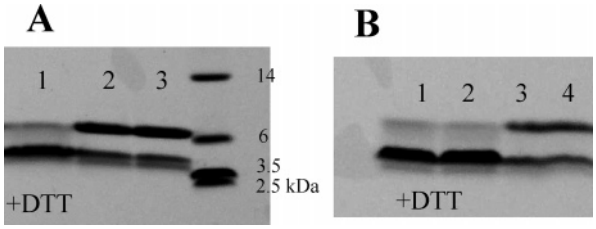

FIGURE 3: Effect of the reducing agent dithiolthreitol (DTT) on the distribution between monomers and dimers in detergents on tricine gels. (A) Results for TM^{370}. Most of the peptides run as monomers in the presence of DTT (lane 1); only a weak dimeric band is observed. This result is similar to results for the wild-type FGFR3 TM domain in the presence of DTT (*10*, *15*). In the absence of DTT (lanes 2 and 3), the dimeric band is stronger than the monomeric band, indicative of disulfide bond-mediated dimer stabilization under nonreducing conditions. (B) Results for TM^{375}. While the dimeric fraction is small in the presence of DTT (lanes 1 and 2), the intensity of the dimer fraction increases in the absence of DTT. Increase of dimer fraction under nonreducing conditions was also observed for TM^{371} (results not shown). Long incubation times at high pH or the addition of the oxidation catalyst $CuSO_4$ (*16*) does not affect the extent of dimerization in the absence of a reducing agent.

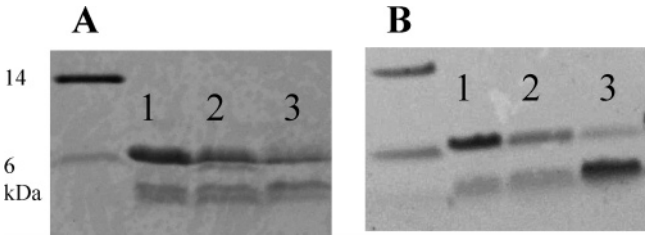

FIGURE 4: Comparison of dimer fractions for the three peptides under nonreducing conditions (no DTT present). (A) Tricine gel. Lane 1, TM^{370}; lane 2, TM^{371}; lane 3, TM^{375}. (B) NuPage gel. Lane 1, TM^{370}; lane 2, TM^{371}; lane 3, TM^{375}. Gels were run as described in Materials and Methods. We observed the highest dimer fraction for TM^{370} and the lowest dimer fraction for TM^{375}.

state (Figure 3A). This is consistent with the expectation of increased dimerization of this mutant due to the formation of disulfide bonds which stabilize the dimeric state (*8*). The low intensity of the dimeric band under reducing conditions is consistent with the formation of a weak TM domain dimer, stabilized by van der Waals knob-into-hole packing interactions, identical to the wild-type FGFR3 TM domain (*11*).

The dimerization of the 375 mutant was also more significant in the absence than in the presence of the reducing agent (Figure 3B); similar results were obtained for the 371 mutant (not shown).

As seen in Figure 3, a fraction of the peptide was monomeric even under nonreducing conditions. The dimer fraction did not increase if the oxidation catalyst $CuSO_4$ was added to the samples, or if the samples were incubated overnight at pH 10. These results demonstrate that dimers form readily in detergent. The fact that dimerization is not 100% under oxidizing conditions can be explained by either (1) oxidation of some of the SH groups to SO_3, such that they lose their disulfide bonding capabilities, or (2) the establishment of an apparent equilibrium between monomers and dimers on the gel. Mass spec of peptides before and after $CuSO_4$ incubation shows no difference in mass (results not shown), such that the SDS−PAGE results likely report on an apparent equilibrium between monomers and dimers

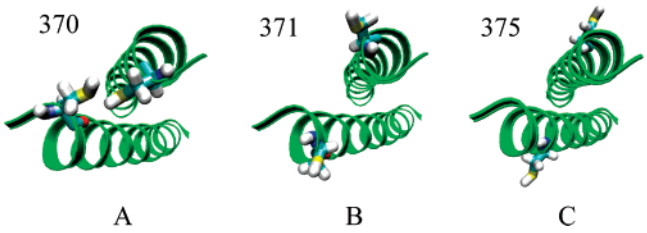

FIGURE 5: Molecular models of the TM^{370} (A) , TM^{371} (B), and TM^{375} (C) dimers, created from the published wild-type dimer model (*11*) by substituting amino acids 370, 371, and 375 with cysteines. In these structures, the distance between the cysteines is the smallest in TM^{370}, intermediate in TM^{371}, and the largest in TM^{371}, consistent with the SDS−PAGE results in Figure 4. We argue that disulfide bonds can form between all three pairs of cysteines only if the TM dimer structure in SDS is very flexible (see text).

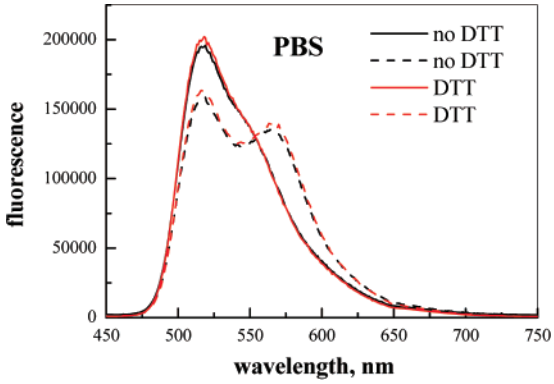

FIGURE 6: Fluorescence spectra of fluorescein/rhodamine labeled $TM^{370/396}$ peptide. Total peptide concentration was 0.2 mol %, donor-to-acceptor ratio was 1:1. Spectra were measured for samples containing fluorescein (donor) and rhodamine (acceptor) labeled peptides (dashed lines), as well as control samples containing only fluorescein-labeled peptides (solid lines). Results in the absence and presence of DTT are shown in black and red, respectively. In the experiments, lipids, fluorescein-labeled and rhodamine-labeled peptides were premixed in organic solvent, the solvent was evaporated, and the samples were hydrated. After hydration, the samples were freeze−thawed three times to achieve full equilibration. The excitation was fixed at 439 nm, such that only fluorescein was directly excited. The emission was scanned from 450 to 750 nm. FRET is manifested by a decrease in fluorescein fluorescence (around 520 nm). The spectra are identical in the presence and absence of DTT in phosphate buffer (shown here), Tris buffer (not shown), or Tris buffer with $CuSO_4$ (not shown). In all cases, the measured dimer fraction for 0.2 mol % peptide was 0.2 ± 0.03, identical to the wild-type dimer fraction under the same conditions (*11*). Thus, no disulfide bonds form in lipid bilayers.

(both disulfide bonded and non-disulfide bonded) in the absence of a reducing agent.

Results, similar to the ones shown in Figure 3, were observed for the NuPage gels. A weak dimer band was observed under reducing conditions; the dimer band was stronger in the absence of a reducing agent. The addition of $CuSO_4$ or long sample incubation at pH 10 prior to gel loading did not affect the results in the absence of DTT.

Next, the relative dimerization propensities of the three mutants, as reported by the maximum amount of dimer, were compared under nonreducing conditions. Figure 4A shows the results for tricine gels. Figure 4B shows the results for Bis-Tris gels. On both gels, the dimer fraction was largest for TM^{370}, intermediate for TM^{371}, and smallest for TM^{375}.

Molecular Modeling of Dimer Structures. Molecular models of the three Cys mutants were produced as described in Materials and Methods and are shown in Figure 5. The helical backbones are shown as green ribbons, and the cysteines are highlighted using a ball-and-stick representation. The TM^{370} model in Figure 5A demonstrates that the two cysteines in the TM^{370} dimer are close to each other, and these cysteines are therefore likely to participate in disulfide bond formation. The distance between the two cysteines is greater in the TM^{371} dimer than in the TM^{370} dimer (Figure 5B). The two cysteines in the TM^{375} dimer are far apart and do not face the dimer interface. Therefore, they should exhibit the lowest probability for disulfide bond formation. Thus, the molecular models appear to be consistent with the SDS gel results shown in Figure 4. Yet, the finding that disulfide bonds form in all three mutant dimers, including the ones with cysteines facing away from the dimer interface, is surprising. We argue that disulfide bonds can form within the context of the dimer structure shown in Figure 5 only if the dimer structure is very flexible. Thus, the observed disulfide bonds should be interpreted as an indication of a high conformational flexibility of the TM dimer structure in detergent. Such high flexibility is probably characteristic of weak dimers in detergent, and is expected to be much lower for strong dimers such as glycophorin A (*24*).

Förster Resonance Energy Transfer (FRET) Studies of the 370 Mutant in Liposomes. FRET can be used to probe the dimerization of TM helices in liposomes, an environment that mimics the biological membrane (*17*). FRET involves the nonradiative transfer of energy from the excited state of a donor to an appropriate acceptor (*25*−*29*), and is widely used for detecting molecular interactions in membranes. In a TM domain dimer, the donor and the acceptor are in close contact (within 10−20 Å) and FRET can be easily detected as a decrease in donor fluorescence and an increase in acceptor fluorescence (*27*−*29*). We have shown that FRET can be used to calculate dimer fractions as a function of protein concentration (protein-to-lipid ratio), as well as the free energy of dimerization of TM helices in bilayers (*17*, *30*). We have demonstrated a weak dimerization propensity for wild-type FGFR3 TM domain (*10*), and we have characterized two mutants: the Ala391→Glu mutant, known as the cause for Crouzon syndrome with acanthosis nigricans (*31*), and the Gly380→Arg mutant, which has been associated with achondroplasia (*18*) just as the Gly375→Cys mutant studied here.

To determine the propensity for Cys370-mediated disulfide bond formation in bilayers, we measured the dimerization propensity of $TM^{370/396}$ in POPC bilayers using a well-characterized FRET pair: fluorescein/rhodamine (*11*). The dyes were attached to Cys396 in $TM^{370/396}$, as described in Materials and Methods. Lipids and peptides were mixed in organic solvent, the solvent was removed completely, and the mixtures were hydrated in buffer (either phosphate buffer or Tris, pH = 7). FRET spectra, acquired for 0.2 mol % total protein concentration (peptide-to-lipid ratio 1:500), are shown in Figure 6. From these spectra, one can calculate the dimer fraction, as discussed in Materials and Methods, and compare it to previous measurements of the wild-type dimer fraction under identical conditions. The calculated dimer fraction for 0.2 mol % $TM^{370/396}$ was 0.2 ± 0.03, and

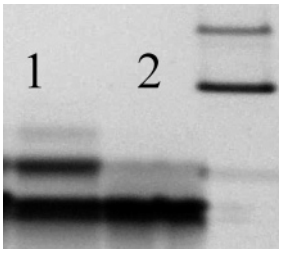

FIGURE 7: SDS−PAGE results for $TM^{370/396}$ in the presence (lane 2) and absence (lane 1) of reducing agent (DTT). In the presence of DTT (lane 2) only a weak dimeric band is observed. In the absence of DTT (lane 1), the dimeric band is much stronger. The addition of $CuSO_4$ did not increase the dimer fraction in the absence of DTT (not shown). Thus, under nonreducing conditions, disulfide-bonded dimers are readily formed on the gel. This indicates that $TM^{370/396}$ is capable of forming disulfide bonds in detergents, but not in bilayers (see Figure 5). A weak trimer can be detected in the absence of DTT, most probably due to the incomplete capping of Cys396 with fluorescent dyes and *N*-ethylmaleimide (see Materials and Methods).

was identical to a previously reported value for the wild-type FGFR3 TM domain at this peptide-to-lipid ratio (*11*). This comparison shows that the $TM^{370/396}$ dimer behaves as wild-type in liposomes. The addition of the oxidation catalyst $CuSO_4$ during sample preparation, prior to hydration of lipids and peptides in buffer, did not affect the results. Therefore, Cys370-mediated disulfide bonds do not form between the two helices in lipid bilayers and do not stabilize the dimer.

To further demonstrate that disulfide bonds did not form, we added DTT to the liposomal samples at a final concentration of 5 mM. We freeze−thawed the samples 5 times, and measured the FRET spectra over the course of several days. The FRET spectra before and after DTT addition were identical, and did not change with time.

The finding that no disulfide bonds form in bilayers appears surprising in view of the close proximity of the cysteines in the TM^{370} structure (Figure 5A). This structure, however, is only a model based on a conformational search in vacuum (see Materials and Methods), and the observed absence of disulfide bonds in $TM^{370/396}$ suggests that the two cysteines are probably further apart than shown in Figure 5A.

The absence of Cys370-mediated disulfide bonds in liposomes, but not in detergent, further suggests that the TM helices in the liposomes are constrained by the highly anisotropic lipid bilayer and their structure is rather rigid. As a result, the probability for disulfide bond formation is greatly reduced.

To study if disulfide bond-stabilized dimers of $TM^{370/396}$ form in detergent, we subjected $TM^{370/396}$ to SDS−PAGE. Results are shown in Figure 7. In the presence of the reducing agent, a weak dimer band is observed. In the absence of the reducing agent, a much stronger dimer band is observed, similar to the results for TM^{370}. The addition of the oxidation catalyst $CuSO_4$ did not increase the dimer fraction. Thus, disulfide bonds readily form in the $TM^{370/396}$ dimer in detergent, just as in TM^{370}, TM^{371}, and TM^{375}. Note that a weak trimeric band can be observed on the gel under nonreducing conditions, which is most probably due to disulfide-bonded trimers, with both Cys370 and Cys396 participating in disulfide bonding. Such trimers could form due to incomplete capping of Cys396 (see Materials and Methods).

DISCUSSION

Overview of Results. We find that, in detergents, disulfide bonds form easily within dimers of TM^{370}, TM^{371}, and TM^{375}, as evident from the differences in dimer band intensities on SDS gels in the presence and absence of reducing agents. We further find that, in the absence of a reducing agent, TM^{370} dimerizes more than TM^{371}, which in turn dimerizes more than TM^{375}. TM^{370} and TM^{371} are associated with the lethal (thanatophoric) dysplasia, while TM^{375} is associated with a much milder dwarfism phenotype, achondroplasia. Thus, the intensities of the dimeric bands appear to correlate with the severity of the phenotype.

The dimer models shown in Figure 5 provide a structural explanation for these observations, because the intensities of the dimeric bands correlate with the distance between the two cysteines in the models. The models further suggest that the TM dimer structure in detergent is very flexible, because disulfide bonds can form between distant pairs of cysteines.

In bilayers, the stability of the $TM^{370/396}$ dimer is similar to the stability measured for wild-type, and is not affected by the presence or absence of a reducing agent. Therefore, no Cys370-mediated disulfide bonds form within the $TM^{370/396}$ dimer in bilayers, despite the fact that disulfide bonds form under similar conditions in detergent. These results demonstrate that the nature of the hydrophobic environment plays an important role in defining the structure and flexibility of transmembrane dimers, and reinforce the view that the dimer structure in detergents is characterized by a very high degree of conformational flexibility.

Results from Cellular Studies. Pathogenic Cys FGFR3 TM domain mutations have been proposed to induce disulfide-mediated stabilization of the active dimeric state of FGFR3 and FGFR3 constitutive activation (*8*, *32*). The effect of the Cys mutations on FGFR3 dimerization and activation in 293T cells was studied by Yayon and colleagues (*32*). In these studies, the activity of the wild-type and the mutants was monitored by measuring phosphorylation of the receptors, as well as the activation of downsteam signaling proteins and genes. The authors found that, in 293T cells, the mutant FGFR3 receptors exhibited spontaneous, ligand-independent dimerization and increased basal phosphorylation, while the wild-type FGFR3 dimerized and was phosphorylated and activated only on FGF stimulation. The Gly370→Cys and Gly371→Cys mutants showed high levels of mitogen-activated protein kinase phosphorylation, while the activation of the Gly375→Cys mutant was lower. The extent of dimerization in the absence of ligand also correlated with the severity of the phenotype. It was strong for Cys370 and Cys371, intermediate for Cys375, and negligible for the wild-type.

Molecular Mechanism behind Pathogenesis. Here we reconcile our results with the findings of Yayon and colleagues, and we put forward a model for the molecular mechanism of Cys-mediated pathogenesis.

Models of RTK activation, including FGFR3 activation, have been proposed based on solved structures of RTK extracellular domains (*1*, *2*, *33*). In the RTK monomer, an equilibrium is believed to exist between two conformations of the extracellular domain: a closed autoinhibited conformation (which prevents dimerization from occurring) and an open conformation, which favors dimerization (*34*). The

extracellular domain in the monomer "flickers" between the closed and the open conformation. Dimerization occurs when two monomers in the open conformation encounter each other. It can be therefore expected that the flickering persists during the dimerization process, and the extent of the flickering directly affects the equilibrium between monomers and dimers in the absence of the ligand (*8*). Finally, ligand binding stabilizes the dimer by stabilizing the open conformation of the extracellular domain.

We propose that the flickering motions associated with transitions between the open and the closed conformation of the extracellular domain are transmitted to the TM domain. Thus, the structure of the TM domain in the context of the monomeric receptor in the plasma membrane is much more dynamic than the structure of the isolated TM domain in liposomes, and approaches the conformational flexibility of the TM domain in detergents. We further propose that disulfide bonds can form between two flickering receptors in close proximity, even in the absence of ligand. These disulfide bonds stabilize the dimeric state of the receptor, which ultimately leads to receptor overactivation and unregulated signaling.

In summary, we propose a conformational flexibility mechanism for the stabilization of the FGFR3 mutant dimers in achondroplasia and thanatophoric dysplasia. The novel aspect of the proposed mechanism is that the dynamic behavior of the receptors is a prerequisite for the disulfide bond-induced FGFR3 overactivation and for disregulated FGFR3 signaling.

REFERENCES

1. Schlessinger, J. (2000) Cell signaling by receptor tyrosine kinases, *Cell 103*, 211−225.
2. Schlessinger, J. (2002) Ligand-induced, receptor-mediated dimerization and activation of EGF receptor, *Cell 110*, 669−672.
3. Lemmon, M. A., Bu, Z. M., Ladbury, J. E., Zhou, M., Pinchasi, D., Lax, I., Engelman, D. M., and Schlessinger, J. (1997) Two EGF molecules contribute additively to stabilization of the EGFR dimer, *EMBO J. 16*, 281−294.
4. Spivakkroizman, T., Lemmon, M. A., Dikic, I., Ladbury, J. E., Pinchasi, D., Huang, J., Jaye, M., Crumley, G., Schlessinger, J., and Lax, I. (1994) Heparin-Induced Oligomerization of Fgf Molecules Is Responsible for Fgf Receptor Dimerization, Activation, and Cell-Proliferation, *Cell 79*, 1015−1024.
5. Lemmon, M. A., and Schlessinger, J. (1994) Regulation of Signal-Transduction and Signal Diversity by Receptor Oligomerization, *Trends Biochem. Sci. 19*, 459−463.
6. Lemmon, M. A., and Engelman, D. M. (1994) Specificity and promiscuity in membrane helix interactions, *Q. Rev. Biophys. 27*, 157−218.
7. Bennasroune, A., Fickova, M., Gardin, A., Dirrig-Grosch, S., Aunis, D., Cremel, G., and Hubert, P. (2004) Transmembrane peptides as inhibitors of ErbB Receptor Signaling, *Mol. Biol. Cell 15*, 3464−3474.
8. Li, E., and Hristova, K. (2006) Role of receptor tyrosine kinase transmembrane domains in cell signaling and human pathologies, *Biochemistry 45*, 6241−6251.
9. Mendrola, J. M., Berger, M. B., King, M. C., and Lemmon, M. A. (2002) The single transmembrane domains of ErbB receptors self-associate in cell membranes, *J. Biol. Chem. 277*, 4704−4712.
10. Li, E., You, M., and Hristova, K. (2005) SDS-PAGE and FRET suggest weak interactions between FGFR3 TM domains in the absence of extracellular domains and ligands, *Biochemistry 44*, 352−360.
11. Li, E., You, M., and Hristova, K. (2006) FGFR3 dimer stabilization due to a single amino acid pathogenic mutation, *J. Mol. Biol. 356*, 600−612.
12. Vajo, Z., Francomano, C. A., and Wilkin, D. J. (2000) The molecular and genetic basis of fibroblast growth factor receptor3 disorders: The achondroplasia family of skeletal dysplasias, Muenke craniosynostosis, and Crouzon syndrome with acanthosis nigricans, *Endocr. Rev. 21*, 23−39.
13. Webster, M. K., and Donoghue, D. J. (1996) Constitutive activation of fibroblast growth factor receptor 3 by the transmembrane domain point mutation found in achondroplasia, *EMBO J. 15*, 520−527.
14. Shiang, R., Thompson, L. M., Zhu, Y.-Z., Church, D. M., Fielder, T. J., Bocian, M., Winokur, S. T., and Wasmuth, J. J. (1994) Mutations in the transmembrane domain of FGFR3 cause the most common genetic form of dwarfism, achondroplasia, *Cell 78*, 335−342.
15. Iwamoto, T., You, M., Li, E., Spangler, J., Tomich, J. M., and Hristova, K. (2005) Synthesis and initial characterization of FGFR3 transmembrane domain: Consequences of sequence modifications, *Biochim. Biophys. Acta 1668*, 240−247.
16. Takagi, T., and Isemura, T. (1964) Accelerating Effect of Copper Ion on Reactivation of Reduced Taka-Amylase A Through Catalysis of Oxidation of Sulfhydryl Groups, *J. Biochem.* 56, 344-&.
17. You, M., Li, E., Wimley, W. C., and Hristova, K. (2005) FRET in liposomes: measurements of TM helix dimerization in the native bilayer environment, *Anal. Biochem. 340*, 154−164.
18. You, M., Li, E., and Hristova, K. (2006) The achondroplasia mutation does not alter the dimerization energetics of FGFR3 transmembrane domain, *Biochemistry 45*, 5551−5556.
19. Adams, P. D., Arkin, I. T., Engelman, D. M., and Brünger, A. T. (1995) Computational searching and mutagenesis suggest a structure for the pentameric transmembrane domain of phospholamban, *Nat. Struct. Biol. 2*, 154−162.
20. Adams, P. D., Engelman, D. M., and Brünger, A. T. (1996) Improved prediction for the structure of the dimeric transmembrane domain of glycophorin A obtained through global searching, *Proteins 26*, 257−261.
21. Brunger, A. T., Adams, P. D., Clore, G. M., DeLano, W. L., Gros, P., Grosse-Kunstleve, R. W., Jiang, J.-S., Kuszewski, J., Nilges, M., Pannu, N. S., Read, R., Rice, L. M., Simonson, T., and Warren, G. L. (1998) Crystallography and NMR system: a new software suite for macromolecular structure determination, *Acta Crystallogr. D 54*, 905−921.
22. Humphrey, W., Dalke, A., and Schulten, K. (1996) VMD: Visual molecular dynamics, *J. Mol. Graphics 14*, 33.
23. Merzlyakov, M., Chen, L., and Hristova, K. (2007) Studies of Receptor Tyrosine Kinase Transmembrane Domain Interactions: The EmEx-FRET Method, *J. Membr. Biol. 215*, 93−103.
24. MacKenzie, K. R., Prestegard, J. H., and Engelman, D. M. (1997) A transmembrane helix dimer: Structure and implications, *Science 276*, 131−133.
25. Wu, P., and Brand, L. (1994) Resonance energy transfer: Methods and applications, *Anal. Biochem. 218*, 1−13.
26. Kenworthy, A. K., Petranova, N., and Edidin, M. (2000) High-resolution FRET microscopy of cholera toxin B-subunit and GPI-anchored proteins in cell plasma membranes, *Mol. Biol. Cell 11*, 1645−1655.
27. Kenworthy, A. K., and Edidin, M. (1998) Distribution of a glycosylphosphatidylinositol-anchored protein at the apical surface of MDCK cells examined at a resolution of <100 Å using imaging fluorescence resonance energy tranfer, *J. Cell Biol. 142*, 69−84.
28. Clegg, R. M. (1995) Fluorescence resonance energy transfer, *Curr. Opin. Biotechnol. 6*, 103−110.
29. Clegg, R. M. (1996) in *Fluorescence Imaging Spectroscopy and Microscopy* (Wang, X. F., and Herman, B., Eds.) pp 179−252, John Wiley, New York.
30. Merzlyakov, M., Li, E., Casas, R., and Hristova, K. (2006) Spectral Forster resonance energy transfer detection of protein interactions in surface-supported bilayers, *Langmuir 22*, 6986−6992.
31. Meyers, G. A., Orlow, S. J., Munro, I. R., Przylepa, K. A., and Jabs, E. W. (1995) Fibroblast-Growth-Factor-Receptor-3 (Fgfr3) Transmembrane Mutation in Crouzon-Syndrome with Acanthosis Nigricans, *Nat. Genet. 11*, 462−464.
32. Adar, R., Monsonego-Ornan, E., David, P., and Yayon, A. (2002) Differential activation of cysteine-substitution mutants of fibroblast growth factor receptor 3 is determined by cysteine localization, *J. Bone Miner. Res. 17*, 860−868.

33. Schlessinger, J. (2003) Autoinhibition control, *Science 300*, 750−752.
34. Ferguson, K. M., Berger, M. B., Mendrola, J. M., Cho, H. S., Leahy, D. J., and Lemmon, M. A. (2003) EGF activates its receptor by removing interactions that autoinhibit ectodomain dimerization, *Mol. Cell 11*, 507−517.
35. Merzlyakov, M., You, M., Li, E., and Hristova, K. (2006) Transmembrane helix heterodimerization in lipids bilayers: probing the energetics behind autosomal dominant growth disorders, *J. Mol. Biol. 358*, 1−7.

BI700986N